Breakthrough of Lysozyme through an Affinity Membrane of Cellulose-Cibacron Blue

Hsien-Chang Liu and J. R. Fried
Dept. of Chemical Engineering and Polymer Research Center, University of Cincinnati, Cincinnati, OH 45221

The dynamic affinity adsorption of lysozyme through stacked flat-sheet cellulose membranes with immobilized cibacron blue 3GA was studied and compared to three affinity-membrane models: diffusion model to explore the importance of axial and radial diffusion; variation model to study the effects of pore-size distribution or thickness variation; and stack model to investigate the effects of stacking flat-sheet membranes. For the diffusion model, when $Pe_r > 0.1$, radial diffusional resistance is significant, but when $Pe_z < 25$, axial dispersion must be considered. For the variation model, increasing pore-size distribution or nonuniform membrane thickness greatly broadens the breakthrough curve. The stack model shows that the stacking of membranes significantly sharpens the breakthrough curves by averaging out the flow dispersion due to pore-size distribution or thickness variation.

Introduction

In the biotechnology industry, scaleup from laboratory research to industrial practice has been one of the most difficult challenges for the engineer. High-purity products are generally achieved only after complex multistep purification, often terminating with affinity chromatography. Affinity chromatography utilizes the specific association of the target protein (ligate) with the adsorbent (ligand) chemically bound to an affinity support such as crosslinked dextran, polyacrylamide, silica gel, porous glass, cellulose, and oxides of various metals (Ernst-Cabrera et al., 1988).

The throughput of an affinity separation device is governed by the inherent kinetics of ligand-ligate association and by the mass-transfer characteristics of the device. Support matrices with small particle sizes in a conventional packed-bed column offer relatively high throughputs due to their large surface area and short ligand-ligate diffusion distance. However, this device requires relatively high operating pressure. A number of interesting developments has emerged over the past few years to overcome this drawback. These include continuous extraction (Pungor, 1987), affinity cross-flow filtration (Huang et al., 1988), radial-flow (Luong et al., 1987) and magnetically fluidized columns (Burns et al., 1985), affinity expanded beds (Chase and Draeger, 1992), and perfusion chromatography (Afeyan et al., 1990).

An affinity device using microporous membranes as the support matrix with sites on the pore wall for ligand attachment has even better potential to provide higher efficiency since it offers high surface area, reduces the diffusion distance, and requires low operating pressure (Zale et al., 1988; Brandt et al., 1988). These will result in high-volume throughput, high efficiency of ligand utilization, and low cost. This approach can lead to solution of scale-up problems in the purification of biomolecules. Although new, commercial affinity membranes are being developed for the biotechnology industry, fundamental studies of affinity-membrane systems have not kept pace. For these reasons, there is a need to provide fundamental information on the characteristic parameters of affinity-membrane systems, as well as an understanding of the operating parameters governing separation performance.

In this study, an affinity-membrane system using cellulose membranes as the support matrices has been prepared. A ligand of cibacron blue 3GA was bound to the cellulose membranes, and the adsorption behavior of lysozyme through the stacked affinity membranes was investigated. System parameters such as membrane properties and operation conditions were varied to evaluate their effects on the performances of the system. Affinity-membrane models based upon capillary flow were developed to study the effects of axial/radial diffusional resistances, pore-size/thickness variation and stacking flat-sheet membranes.

Correspondence concerning this article should be addressed to J. R. Fried.

Experimental Studies

Materials

Chicken egg lysozyme was purchased from Sigma Chemical Co. Certified-grade sodium chloride, sodium carbonate, sodium bicarbonate, hydrochloric acid, sodium azide, and tris(hydroxymethyl)aminomethane were purchased from Fisher Scientific. Cellulose acetate (E-398-10) was purchased from Eastman Chemical Products. Regenerated cellulose membranes from Micro Filtration Systems Co. were used as the support matrices for the affinity system. Membranes having 0.65- and 3-μm mean pore diameters and 110-μm thickness were used in this study.

Affinity-membrane preparation

The covalent coupling of cibacron blue 3GA dye to the membrane matrix results from the formation of an ether linkage between the triazine ring of the dye and the hydroxyl group of cellulose. First, the membranes were immersed in a 1% (w/v) aqueous solution of cibacron blue 3GA at 60°C while the solution was stirred. Approximately 30 min later, NaCl (60 g/L of the reaction solution) was added to the solution and stirring was continued for 1 h at 60°C. After the solution is heated to 80°C, Na_2CO_3 (20 g/L of the reaction solution) was added to the reactor and the stirring continued at this temperature. After 1 h, the solution was allowed to cool to room temperature and the blue membranes were preserved in a 0.1% sodium azide solution and stored in the refrigerator to minimize bacterial attack.

Affinity operation

An HPLC (high-pressure liquid chromatography) pump (Spectra-Physics, mdl. SP8800) was used to circulate the buffer and protein solution through the affinity-membrane cell. A UV/visible detector (Varian) was used to measure absorbance of the effluent in the UV range at 280 nm. Detector signals were recorded by an IBM personal computer. Tubings and tubing connectors were made of stainless steel or Teflon.

Affinity procedures

The adsorption of lysozyme onto blue membranes was evaluated at room temperature with 10 or 33 pieces of cellulose membranes per batch. Tris-HCl buffer (50 mM Tris-HCl/50 mM NaCl, pH 8.0) was used as the adsorption medium. First, the membranes were equilibrated with the adsorption buffer by pumping the buffer through the affinity cell at a flow rate of 0.2 to 1.5 mL/min for more than 20 min. The buffer solution was then replaced by the ligate solution to begin the adsorption process. The output tubing of the cell was connected to a continuous-flow UV detector to measure absorbance of the effluent at 280 nm. The recorded signals served to determine the breakthrough curve for the system. The HPLC pump was used to control the transmembrane flow rate which was also calibrated by measuring the volume of the effluent solution over 5-min intervals. The adsorption was carried out until the ligate concentration of the effluent reached approximately 85–95% of the initial feed concentration.

After adsorption, the feed solution was replaced by the washing solution buffer. The same buffer that was used in the adsorption step was employed (without ligate) to wash off the unabsorbed protein until the absorbance at 280 nm for the effluent declined to zero. For the cellulose-cibacron blue/lysozyme system, desorption of the lysozyme was obtained by use of 10–20 mL of 500-mM KCl/50-mM Tris HCl buffer at pH 8.0.

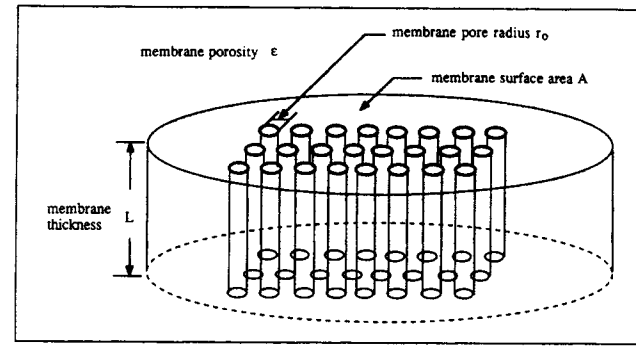

Figure 1. Affinity-membrane model.

Diffusion Model

Model description

In the development of a model for the breakthrough curve of a macroporous affinity membrane, the flow of the ligate solution through the membrane is taken to be equivalent to flow through an array of fine capillaries parallel with one another, as illustrated in Figure 1. The radii of the capillaries are equal and equivalent to the membrane mean pore radius, r_o, while the capillary density is given by the membrane porosity, ϵ. Furthermore, the following assumptions are made to simplify the model: (1) the diffusion coefficient (D), viscosity (μ), and density (ρ) of the ligate solution are constant; (2) the momentum and mass balance equations are not coupled and, therefore, may be solved separately (that is, fluid linear velocity is independent of concentration and varies only with radius); and (3) mass transport may occur by radial diffusion, axial diffusion, and axial convection while other transport mechanisms, such as radial convection or surface diffusion, are negligible.

Based upon the assumptions cited above, a mass balance on the washer-shaped element volume within one capillary yields the following continuity equation:

$$\frac{\partial C}{\partial t} + U\frac{\partial C}{\partial z} = D\frac{1}{r}\frac{\partial}{\partial r}\left(r\frac{\partial C}{\partial r}\right) + D\frac{\partial^2 C}{\partial z^2} \qquad (1)$$

where r is the radial direction, z is the axial (fluid-flow) direction, $C(r,z,t)$ is the concentration of the ligate in the fluid, and $U(r)$ is the linear velocity of the fluid. In order to solve this two-dimensional partial differential equation, the model is further simplified by either neglecting the axial *or* radial diffusion. In the case that both axial and radial diffusion can be neglected, the equation has been solved analytically by Thomas (1967), as discussed below.

Kinetic rate expression

The basis for affinity separations is the formation of a strong

noncovalent bond between the ligand and ligate. Assuming that the adsorbent has a fixed number of equivalent ligands to which ligates bind one to one in a reversible way, the interaction can be described by an equilibrium relationship of the form (Janson and Ryden, 1989):

$$\text{Ligand} + \text{Ligate} \underset{k_d}{\overset{k_a}{\Longleftrightarrow}} \text{Ligand-ligate}$$

On this basis, the affinity adsorption on the pore wall (at $r = r_o$) per unit volume of the liquid phase (g/cm^3 solution), R_a, can be described by the kinetics of the affinity interaction as

$$R_a = -\frac{1-\epsilon}{\epsilon}\frac{\partial q_{gd}}{\partial t} = \frac{1-\epsilon}{\epsilon}\left(k_a C_s q_{gd} - k_d q_{gdt}\right)$$

$$= \frac{1-\epsilon}{\epsilon}\left[k_a C_s\left(q^o_{gd} - q_{gdt}\right) - k_d q_{gdt}\right] \tag{2}$$

where k_a is the associative constant, k_d is the dissociative constant, $C_s(z,t)$ (function of z and t only) is the concentration (g/cm^3 solution) of the ligate at the interface, q_{gd} is the concentration (g/cm^3 matrix) of free ligand, q^o_{gd} is the initial concentration of the ligand, q_{gdt} is the concentration of bound ligand-ligate, and ϵ is the membrane porosity.

Several investigators (Wankat, 1974; Graves and Wu, 1974; and Horstmann et al., 1986) have shown that the equilibrium relationship between the ligand and the ligate can be described by a Langmuir isotherm. At equilibrium, Eq. 2 reduces to the Langmuir model:

$$q^*_{gdt} = q^o_{gd}\frac{C_o}{C_o + K_d} \tag{3}$$

where q^*_{gdt} is the concentration of bound ligand-ligate at equilibrium and K_d is the apparent dissociation equilibrium-constant given by:

$$K_d = \frac{k_d}{k_a} \tag{4}$$

It is further assumed that the flow characteristics for a dilute ligate solution follow Newtonian behavior. For flow of a Newtonian fluid in a circular tube with radius r_o, the velocity distribution $U(r)$ of a laminar flow can be described as a function of the average fluid velocity U_o and radius r (Bird et al., 1960) as:

$$U(r) = 2U_o\left[1 - \left(\frac{r}{r_o}\right)^2\right]. \tag{5}$$

Neglect of axial and radial diffusion

Neglecting both axial and radial diffusion, we have the following partial differential equation in one spatial dimension (z direction only):

$$\frac{\partial C}{\partial t} + U_o\frac{\partial C}{\partial z} = -R_a = \frac{1-\epsilon}{\epsilon}\frac{\partial q_{gd}}{\partial t} \tag{6}$$

where R_a is the interface adsorption rate per unit volume of the liquid phase defined by Eq. 2. The initial condition is given as:

$$C(z,t) = 0 \qquad \text{at } t = 0 \tag{6a}$$

and the boundary condition as:

$$C(z,t) = C_o \qquad \text{at } z = 0. \tag{6b}$$

The analytical solution to this differential equation with the above initial and boundary conditions has been obtained by Thomas (1967). C/C_o as a function of t for a wide range of affinity adsorption procedures can be obtained from integrating the Thomas solution numerically (Chase, 1984; Arnold, 1986; Hiester and Vermeulen, 1952). The breakthrough curves from the Thomas method were compared to the breakthrough curves predicted on the basis of other methods used in this study.

Neglect of axial diffusion

Neglecting the axial diffusional term in Eq. 1 gives:

$$\frac{\partial C}{\partial t} + U\frac{\partial C}{\partial z} = D\frac{1}{r}\frac{\partial}{\partial r}\left(r\frac{\partial C}{\partial r}\right) \tag{7}$$

with the initial condition

$$C(r,z,t) = 0 \qquad \text{at } t = 0 \tag{7a}$$

and boundary conditions

$$\frac{\partial C}{\partial r} = 0 \qquad \text{at } r = 0 \tag{7b}$$

$$C = C_o \qquad \text{at } z = 0 \tag{7c}$$

$$-D\frac{\partial C}{\partial r}A = R_a V \qquad \text{at } r = r_o \tag{7d}$$

where R_a is defined by Eq. 2, r_o is the mean pore radius, A is the membrane surface area, and V is the pore volume. Here, V/A would be equal to $\pi r_o^2 L/2\pi r_o L = r_o/2$.

Dimensionless analysis

We can define the following dimensionless variables:

$$C' = \frac{C}{C_o};\ z' = \frac{z}{L};\ r' = \frac{r}{r_o};\ \theta = \frac{t}{t'};\ t' = \frac{L}{U_o};\ U_o = \frac{Q}{\epsilon A};\ U' = \frac{U}{U_o}$$

Furthermore, we will also define ϕ as the fractional saturation of ligand:

$$\phi = \frac{q_{gdt}}{q^o_{gd}} = 1 - \frac{q_{gd}}{q^o_{gd}}$$

Substituting ϕ into Eq. 2 yields:

$$R_a = -\frac{1-\epsilon}{\epsilon}\frac{\partial q_{gd}}{\partial t} = \frac{1-\epsilon}{\epsilon} q^o_{gd}\left(\frac{\partial \phi}{\partial t}\right)$$

$$= \frac{1-\epsilon}{\epsilon}\left[k_a C_s q^o_{gd}(1-\phi) - k_d q^o_{gd}\phi\right]. \quad (8)$$

Substituting the dimensionless variables into Eq. 1 yields the dimensionless form of the partial differential equation as:

$$\frac{\partial C'}{\partial \theta} + 2(1-r')\left(\frac{\partial C'}{\partial z'}\right) = \frac{1}{Pe_r}\left[\frac{1}{r'}\frac{\partial}{\partial r'}\left(r'\frac{\partial C'}{\partial r'}\right)\right] \quad (9)$$

with the dimensionless initial condition

$$C'(r',z',\theta) = 0 \qquad \text{at } \theta = 0 \quad (9a)$$

and dimensionless boundary conditions

$$\frac{\partial C'}{\partial r'} = 0 \qquad \text{at } r' = 0 \quad (9b)$$

$$C' = 1 \qquad \text{at } z' = 0 \quad (9c)$$

$$\frac{\partial C'}{\partial r'} = -\frac{1}{2} Pe_r\, Ld\, Da \qquad \text{at } r' = 1 \quad (9d)$$

where

$$Pe_r = \frac{\text{characteristic diffusion time}}{\text{residence time}} = \frac{r_o^2/D}{L/U_o}$$

$$Da = \frac{\text{residence time}}{\text{characteristic reaction time}} = \frac{L/U_o}{1/[k_a C_s(1-\phi) - k_d\phi]}$$

$$Ld = \frac{\text{characteristic ligand capacity in the system}}{\text{characteristic ligate quantity in the feed}} = \frac{(1-\epsilon)q^o_{gd}}{\epsilon C_o}$$

Neglect of radial diffusion

Neglecting the radial diffusion, we have the following partial differential equation in one spatial dimension (z-direction only):

$$\frac{\partial C}{\partial t} + U_o\frac{\partial C}{\partial z} = -R_a + D\frac{\partial^2 C}{\partial z^2} \quad (10)$$

with the initial condition

$$C(z,t) = 0 \qquad \text{at } t = 0 \quad (10a)$$

and boundary conditions

$$\frac{\partial C}{\partial z} = 0 \qquad \text{at } z = L \quad (10b)$$

$$U_o C - D\frac{\partial C}{\partial z} = U_o C_o \qquad \text{at } z = 0 \quad (10c)$$

Since the axial diffusion is significant, the Danckwerts boundary condition (Danckwerts, 1953) as shown in Eq. 10c was used here at the entrance of the system ($z = 0$). Substituting dimensionless variables into Eq. 10 yields the dimensionless form of the partial differential equation:

$$\frac{\partial C'}{\partial \theta} + \frac{\partial C'}{\partial z'} = -Ld\, Da + \frac{1}{Pe_z}\frac{\partial^2 C'}{\partial z'^2} \quad (11)$$

with the initial condition

$$C'(z',\theta) = 0 \qquad \text{at } \theta = 0 \quad (11a)$$

and boundary conditions

$$\frac{\partial C'}{\partial z'} = 0 \qquad \text{at } z' = 1 \quad (11b)$$

$$\frac{1}{Pe_z}\frac{\partial C'}{\partial z'} = C' - 1 \qquad \text{at } z' = 0 \quad (11c)$$

where

$$Pe_z = \frac{\text{characteristic diffusion time}}{\text{residence time}} = \frac{L^2/D}{L/U_o}$$

In this model, the affinity-membrane system can be characterized by four dimensionless numbers—Pe_r, Pe_z, Ld, and Da—which are defined by the *system properties* (diffusion coefficient of the ligate D and initial concentration of the ligand q^o_{gd}); *membrane properties* (porosity ϵ, thickness L, and mean pore radius r_o), *affinity kinetics* (associative constant k_a and dissociative constant k_d), and the *operational parameters* (feed mass-flow rate Q and feed ligate concentration C_o). Pe_r is a measure of the radial diffusional resistance of the system at a certain operation condition while Pe_z represents the axial dispersion resistance of the system. Da is related to the efficiency of the adsorption interaction and Ld is a measure of the system capacity with respect to the feed ligand concentration.

Implicit finite difference methods (Carnahan et al., 1969) were used to solve the partial differential equations, Eqs. 9 and 11, with the initial and boundary conditions. The programs (Liu, 1993) were written in FORTRAN and run on an IBM 386 personal computer.

Analysis of breakthrough behavior

Most affinity separations are operated in the frontal analysis mode. This includes continuous flow of the ligate solution into the inlet until a breakthrough occurs as indicated by detection of the ligate at the system outlet. The plot of effluent concentration of the ligate vs. time or throughput volume is called the breakthrough curve. Dimensionless breakthrough curves where dimensionless effluent concentration are plotted vs. dimensionless effluent volume were used in the model analysis. The dimensionless effluent concentration is the ratio of effluent ligate concentration over feed ligate concentration. The dimensionless effluent volume is the ratio of the amount of ligate introduced to the system over the total system capacity at equilibrium. System parameters and operating parameters were varied one at a time in order to study the effect of each property

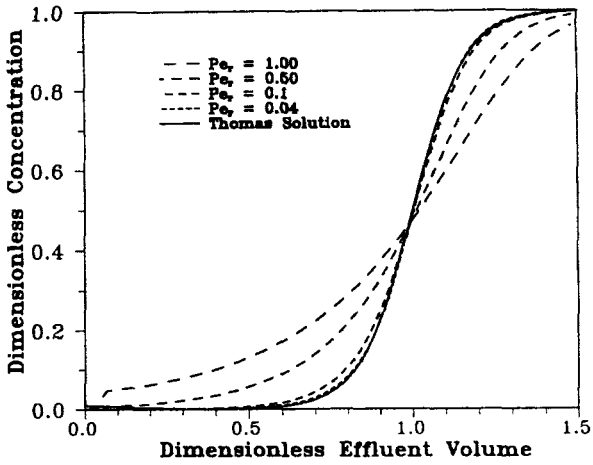

Figure 2. Effect of radial dispersion on the breakthrough curves from the diffusion model.

on the breakthrough behavior of the affinity-membrane processes.

Figure 2 shows the effect of the Peclet number in the r direction, Pe_r, on the breakthrough curves predicted from the diffusion model (with negligible axial diffusion). Pe_r is a measure of the radial diffusional resistance of the system at a certain operating condition. At large Pe_r (for example, $Pe_r = 1$), the radial diffusional resistance is high so that there is a broad concentration profile along the r direction. The concentration of ligate near the membrane surface would be significantly lower which reduces the adsorption rate of the ligate and results in a broad breakthrough curve. When $Pe_r > 0.1$, the radial diffusional resistance is significant while when $Pe_r < 0.04$, the predicted breakthrough curve coincides with the one obtained from the Thomas solution, that is, the radial diffusional resistance is negligible.

Figure 3 shows the effect of the Peclet number in the z direction, Pe_z on the breakthrough curves predicted from the diffusion model (with negligible radial diffusional resistance). Pe_z represents the axial diffusional resistance of the system at a certain operating condition. At low Pe_z, the axial diffusional flux is very high so that concentration of ligate is dispersed

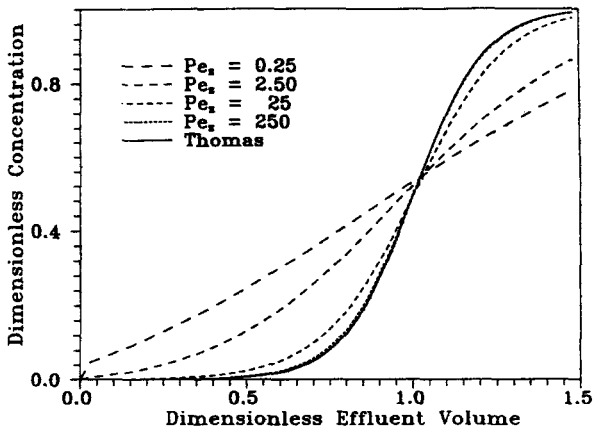

Figure 3. Effect of axial dispersion on the breakthrough curves from the diffusion model.

along the axial direction and this would result in a very broad breakthrough curve. At $Pe_z < 25$, the axial dispersion is significant while at $Pe_z > 250$, the predicted breakthrough curve is essentially the same as the one calculated from the Thomas solution, that is, the axial dispersion effect can be neglected.

The preceding model was developed for a flat-sheet affinity-membrane system. However, it can also apply to other pressure-driven affinity-membrane systems such as hollow fibers. The hollow-fiber configuration may be preferred to a flat-sheet one since it can provide a large surface area in a small module. For example, during the adsorption stage of an affinity operation using hollow fiber membranes as the affinity support, the ligate solution is circulated through the bore side of the fiber. Differential pressure of 30–100 psi (207–689 kPa) is applied across the membrane to push the ligate solution through the porous channels of the membranes to the shell side of the fiber modules. Hollow-fiber systems are particularly useful for treating dilute ligate solution. In the model, membrane pore structure is represented by a bundle of capillaries. The pore diameter of each individual capillary is assumed to remain constant along its path in the membrane. Therefore, the model is not applicable to the system using highly asymmetric membranes with truncated cone shape pores. The cone shape pores are not favorable in the affinity system since some portion of the membrane would have high diffusional resistance (with large pore) and the other would have low diffusional resistance. This nonuniform adsorption efficiency would reduce the overall ligand utilization. Unless the membrane is intended for both concentration (ultrafiltration) and purification (affinity separation) purposes, an asymmetric membrane is not recommended. Membranes prepared from the phase inversion process usually have wide pore-size distribution and vary in thickness. Flow of fluid through microporous membranes in the laminar flow can be related to the pressure across the membrane, solution viscosity, membrane thickness and membrane pore size by the Hagen-Poiseuille equation (Bird et al., 1960). The volumetric flow rate of the solution through each pore is proportional to the fourth power of the pore radius, r_o, and inversely proportional to the membrane thickness. To calculate membrane breakthrough curves as a function of pore-size distribution and thickness variation, the solution of the model can be achieved by solving each set of differential equations with various Pe_z, Pe_r, Ld and Da numbers based on the pore sizes and thickness. The total flow of the ligate solution through all the pores can then be obtained by integrating the flow through individual pores. This involves extensive programming and is planned for future studies.

Experimental Results and System Analysis

In order to provide reproducible breakthrough curves and offer the best opportunity to compare the model predictions with experiment, several module designs were evaluated. In our initial attempt to pack the membrane evenly, a donut-shape spacer (cellulose acetate membrane) was placed between two affinity membranes for sealing. The membranes and spacers were sandwiched between two stainless steel porous supports and two distributors. After loading the cell, the sandwich was pressed so that all the membranes have the same original thickness around the entire membrane area to prevent uneven flow of liquid through the membranes. The affinity

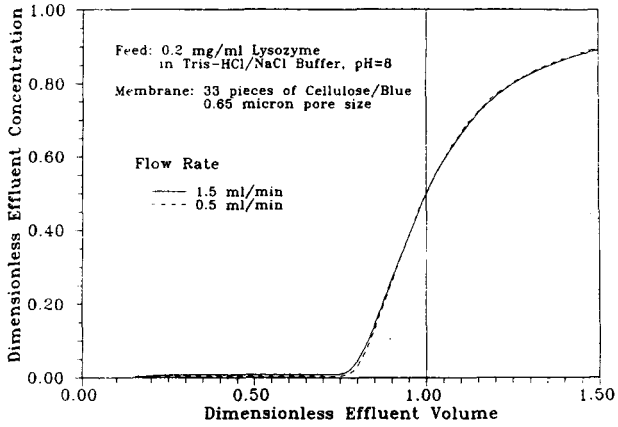

Figure 4. Breakthrough curves of lysozyme through blue membranes with old packing.

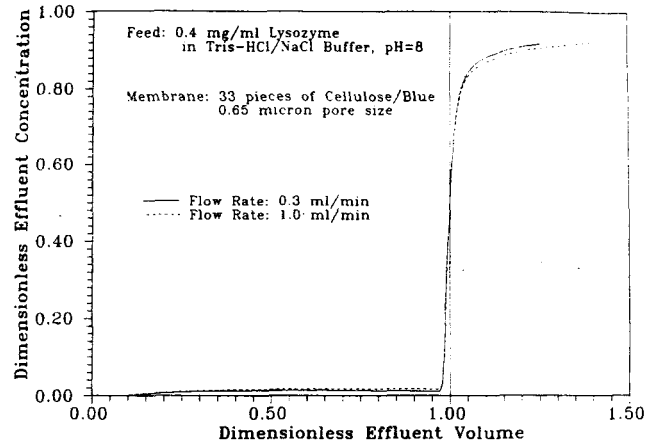

Figure 5. Breakthrough curves of lysozyme through blue membranes with new packing.

cells were made of two pieces of stainless steel holders. Membranes with 25.4 mm in diameter were used. Figure 4 shows the breakthrough curve of lysozyme through 33 pieces of blue membranes having 0.65-μm mean pore diameter. Relatively broad breakthrough curves were observed for an affinity-membrane system with this packing method. The breakthrough curves were not dependent on the feed flow rate. From the model analysis, the broad breakthrough curve could be due to several factors including radial diffusion resistance, axial dispersion, kinetic resistance, and nonideality in column packing. In first three cases, the breakthrough curve would be strongly dependent on the feed flow rate. As the breakthrough curves are nearly independent of flow rates, as shown in Figure 4, it is reasonable to conclude that the packing of the membranes was not an ideal one so that flow of ligate solution through the affinity cell was not uniformly distributed. These may be attributed to the leakage along the side of the membranes, uneven overall thickness of the stacked membranes, and variation of spacer sizes.

To improve the packing, instead of using spacers between membranes to effect the sealing, cellulose acetate solution (10% cellulose acetate in acetone) was used as the sealant. Stacked membranes were sandwiched between two porous supports, two distributors and two acrylic holders. The polymer solution was poured to the side of the sandwich for sealing. After drying, the sealant, cellulose acetate must have shrunk as the total sandwich thickness decreased about 5%. This shrinkage may contribute to the good sealing. As shown in Figure 5, very sharp breakthrough curves were observed for the affinity-membrane system prepared in this way. The same batch of membranes was used as in the previous run with the old packing method. In this case, the breakthrough curves were also not dependent on the feed flow rate. Figure 6 shows breakthrough curves for two different feed concentrations at a fixed flow rate. The same sharp breakthrough curves were obtained and the breakthrough curves were independent of the feed concentration. This demonstrates that the affinity adsorption of the system was not governed by the kinetic rate or diffusion resistance. The result shows that convective flow of ligate through membrane pore structure reduces the diffusion resistance drastically. This is a significant advantage over conventional porous beads for which there is no convective flow through the pores. The deviation of the breakthrough curves near the tear end may be due to the following reasons. The membranes prepared from the phase inversion process may have some dead volume which cannot be reached by convective flow. When membranes are stacked, more dead volume may also be created if the membranes have very rough surfaces. The adsorption of the ligand in the dead volume would be limited by the slow diffusion of the ligate through the dead space. Nonspecific adsorption may also contribute to the slow adsorption rate.

Figure 7 shows the breakthrough curves for stacked membranes with 3-μm mean pore diameters compared to the 0.65-μm mean pore diameters used in the previous studies (that is, Figures 5 and 6). Broader breakthrough curves were observed and the breakthrough curves were also not dependent on the feed flow rate. The dynamic capacity of the system remained relatively constant (decreased from 9.2 to 9.0 mg/cm^3) as the feed flow rate was increased from 0.2 to 1.5 mL/min. This means that an increase in the throughput volume of the operation would not be at expense of the system capacity or ligand utilization. The reason why the breakthrough curves from 3-μm membranes were broader than breakthrough curves from 0.65-μm membranes could be attributed to the pore-size

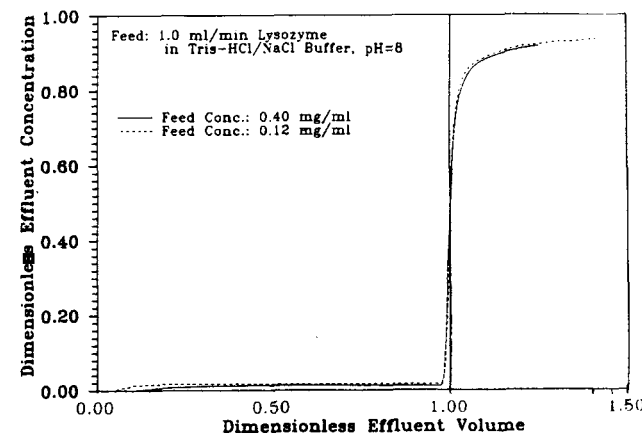

Figure 6. Effect of feed concentration on the breakthrough curves.

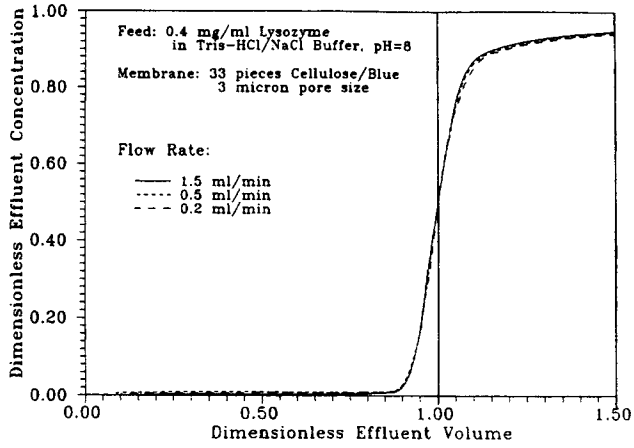

Figure 7. Breakthrough curves of lysozyme through blue membranes (3-μm pore size).

distribution. It is suspected that 3-μm membranes have wider pore-size distribution.

Variation Model

Calculation of breakthrough curves with pore-size distribution

Most polymeric microporous membranes are produced by the method of the phase-inversion process. Membranes produced from this process generally have wide pore-size distribution and some thickness variation. Fluid flow through a microporous membrane in the laminar region can be expressed by the Hagen-Poiseuille equation (Bird et al., 1960):

$$Q_v = \frac{\pi \Delta P r_o^4}{8 \mu L} \tag{12}$$

where Q_v is the volumetric flow rate, r_o is the pore radius, ΔP is the pressure difference across the membrane, μ is the solution viscosity and L is the membrane thickness.

The volumetric flow rate of the solution through each pore is proportional to r_o^4. It is assumed that pressure difference across the membrane and solution viscosity are constant and that the membranes have uniform porosity and ligand density.

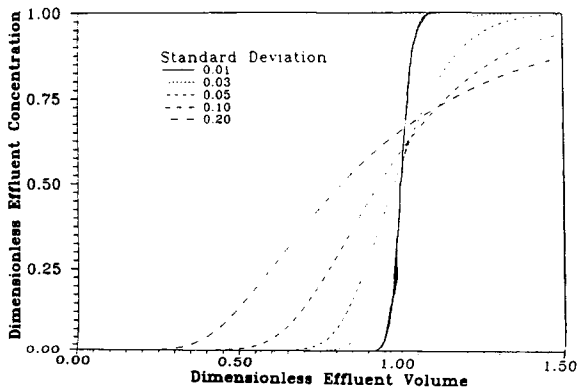

Figure 8. Effect of pore-size distribution on the breakthrough curves.

Radial/axial diffusion and kinetics of the affinity interaction are neglected. For one affinity-membrane system with known pore-size distribution, the breakthrough curves of the system can be calculated. Membranes with pore size of normal distribution are used as examples to demonstrate the effect of pore-size distribution on the affinity system. For membranes of mean pore radius r_o and pore variation expressed in terms of the standard deviation, σ, from the mean value the fraction of membrane pores with pore radius of r can be calculated by the following relation (Miller and Freund, 1985):

$$f(r) = \frac{1}{\sqrt{2\pi}\sigma} \exp(-z^2/2) \qquad \text{where } z = \frac{r - r_o}{\sigma} \tag{13}$$

From the Hagen-Poiseuille equation where the flow rate is proportional to r^4, the residence time of fluid through a membrane with a pore radius r would *be inversely* proportional to r^4. Also, the capacity of the membranes is proportional to the surface area of the membrane pore ($=2\pi rL$) which is proportional to the membrane pore radius r. Therefore, from the residence time and the membrane capacity, the time required for pores with radius r to reach saturation can be calculated. The breakthrough curves for affinity membranes with known pore-size distribution can then be constructed by integrating the breakthrough for every pore (Liu, 1993). As shown in Figure 8, the breakthrough curves broaden significantly as the pore-size distribution increases. Even at standard deviation of 0.03, the effect of pore-size distribution cannot be neglected. With 0.03 standard deviation, 99% of the membrane pores are within 10% of the membrane mean pore size (Miller and Freund, 1985). This is a very narrow pore-size distribution for phase inversion membranes. This model is applicable to both the flat-sheet affinity-system (with single piece of membranes), as well as the hollow-fiber system.

Calculation of breakthrough curves with thickness variation

A similar program was written based on the Hagen-Poiseuille equation where the flow rate is inversely proportional to the membrane thickness. Furthermore, the capacity of the membranes is proportional to the membrane thickness. Therefore, the time required for pores with thickness L to reach saturation is proportional to L^2. From this relation, the breakthrough curves for affinity membranes with known thickness variation can be calculated (Liu, 1993). Figure 9 shows the effect of increasing standard deviation of the mean thickness on the breath of the breakthrough curve. The breadth of the breakthrough curve increases with increasing standard deviation but to a slightly smaller extent than predicted for pore-size distribution. The effect of the thickness variation is quite significant. Since commercial microporous membranes are typically quite uniform in thickness, it is expected that the pore-size distribution would be the controlling morphological factor influencing the breadth of the breakthrough curve.

Stack Model

Calculation of breakthrough curves with stacked membranes

An affinity system using stacked membranes in this study

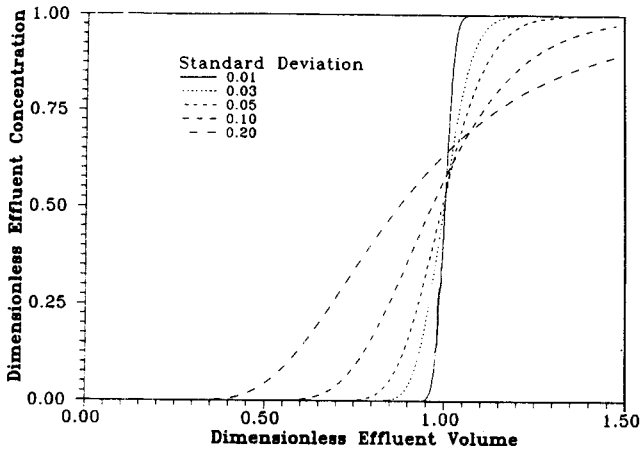

Figure 9. Effect of thickness variation on the breakthrough curves.

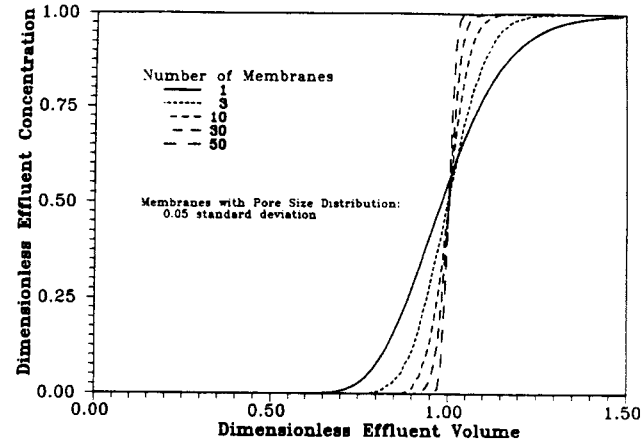

Figure 10. Effect of stacking membranes on the breakthrough curves (theoretical).

has a considerably sharper breakthrough curve than one using hollow fibers, as shown by data from Kim et al. (1991) and from Iwata et al. (1991). This behavior can be explained on the basis of the following analysis. For hollow fiber membranes, the broad breakthrough curves can be attributed to the following four factors: pore-size distribution; variation in the fiber wall thickness (eccentricity on hollow fibers); a decrease in radial velocity due to a decrease in axial pressure drop along the fiber lumen; and dispersion due to the entrance and exit effects from large system volume in the lumen and shell sides of the fibers. The dispersion due to the entrance and exit effects for flat-sheet membranes can be minimized by stacking membranes to increase the total system volume so that the entrance and exit effects are relatively negligible. Furthermore, the pore-size distribution and thickness variation of the membranes are effectively averaged out by stacking of about 30 pieces of membranes. The effect is very significant so that the flow distribution through the membrane system is highly uniform. To calculate the breakthrough curves of one affinity system with stacked membranes, it is assumed that membranes have uniform porosity, uniform ligand density and pore sizes of normal distribution. Radial/axial diffusion and kinetics of the affinity interaction are neglected and the Hagen-Poiseuille equation is applicable. It is assumed that all the membrane pores are stacked orderly without channeling and that each pore would connect one after the other. If, for example, each piece of membranes has n pores, then m pieces of membrane would provide a total of $m \times n$ pores. These pores are arranged randomly to produce n separate flow paths. A FORTRAN program was written to calculate the breakthrough curves of affinity-membrane systems with known pore-size distribution and a specified number of stacked membranes (Liu, 1993). First, from Eq. 13, pore sizes are assigned to each pore (from the first pore $i=1$ to the last pore $i=n$ for each membrane) in every membrane (from $j=1$ to $j=m$). Using random number generator from the FORTRAN utility function, one set of m random integer numbers ranging from 1 to n is generated and these numbers are assigned one by one to the first aligned stacked pores (m stacked pores) in the first flow path, followed by successive sets of m random numbers (excluding the numbers being picked before) to define pore sizes for the next 2 to n flow paths. The residence time of each flow path can be calculated using the relation from the Hagen-Poiseuille equation. The flow rate through one flow path comparing to the flow rate through other flow paths is proportional to the summation of $(1/r_i^4)$ from pore 1 ($i=1$) to pore n ($i=n$) in that particular flow path. Since the capacity is proportional to the surface area ($2\pi rL$) and L is constant, the total capacity of each flow path is proportional to the summation of r_i from pore 1 to pore n in that particular flow path. From the flow rate and the capacity of each path, the time required for each path to reach saturation can be calculated. The breakthrough curves can then be constructed by summarizing breakthrough information for these n flow paths. Setting the number of pores to 1,000 is sufficient to produce smooth breakthrough curves. Figure 10 shows the effect of stacking membranes on the breakthrough curves. As more membranes are stacked, the breakthrough curves become much sharper. This averaging effect is very dramatic when only a few membranes are stacked. As more membranes are stacked (more than 40 pieces), adding more membranes would not increase the sharpness of the breakthrough curves significantly. As shown by the experimental data in Figure 11, the breakthrough curve obtained by stacking 33 membranes with 3-μm pore size is much sharper than the one obtained by using only 10 membranes.

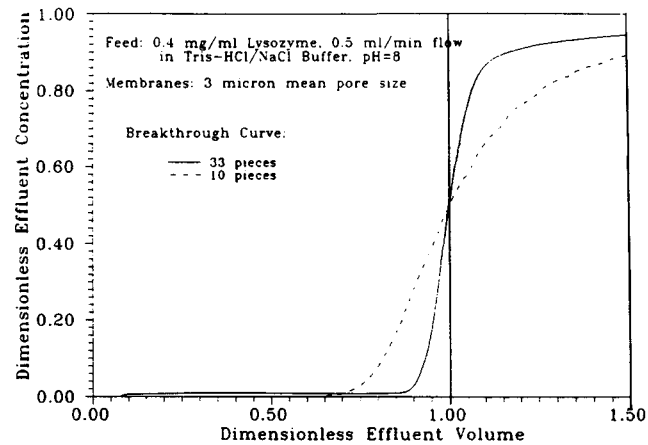

Figure 11. Effect of stacking membranes on the breakthrough curves (experimental).

Conclusions

In the diffusion/kinetics model, the affinity system was characterized by three dimensionless numbers: Peclet number (Pe_r or Pe_z), Ligand number (Ld) and Damköhler number (Da). These are defined by the *system properties* (that is, the diffusion coefficient of the ligate and the initial concentration of the ligand); *membrane properties* (that is, membrane porosity, thickness and mean pore radius), *affinity kinetics* (associative and dissociative rate constant) and *operational parameters* (that is, feed mass flow rate and feed ligate concentration). Pe_r is a measure of the radial diffusional resistance of the system at a certain operation condition while Pe_z represents the axial diffusion resistance of the system. From the model analysis, it can be concluded that when $Pe_r > 0.1$, the radial diffusional resistance is significant and that when $Pe_z < 25$, the axial dispersion cannot be neglected. In order to completely prevent axial dispersion or eliminate radial diffusion resistance, it is necessary to operate the affinity-membrane system at a condition of $Pe_z > 250$ or $Pe_r < 0.04$, respectively.

From the variation analysis, the effects of pore-size distribution and thickness variation for a hollow-fiber system or flat-sheet membrane system (single piece membrane) are very significant. These effects can be reduced by stacking membranes to average out the dispersion. Therefore, an affinity system using stacked membranes would have a considerably sharper breakthrough curve than the affinity system with hollow fibers. From the experimental results (the breakthrough curves are not dependent on the residence time or flow rate over 0.2–3.0 mL/min) and the model analysis ($Pe_r < 0.04$, $Pe_z > 250$), the radial diffusional resistance and axial dispersion for stacked membranes (33 pieces or 10 pieces) with pore sizes of 0.65 and 3 μm can be neglected. From the experimental results, it can be concluded that the adsorption kinetics between lysozyme and cellulose/blue membranes is not the limiting resistance under current operating conditions. From the stack model, the effect of stacking membranes on the breakthrough curves is very significant. As more membranes are stacked, the breakthrough curves become much sharper. This is in agreement with the experimental results that the breakthrough curve from 33 pieces of stacked membranes with 3-μm pore size is much sharper than the one using 10 stacked pieces of the same membranes.

Notation

A = membrane surface area, cm^2
C = concentration of the ligate in the fluid, g/cm^3
C_o = ligate concentration in the feed, g/cm^3
C' = dimensionless concentration
C_s = ligate concentration at the interface, g/cm^3
q_{gd} = concentration of free ligand, g/(cm^3 matrix)
q^o_{gd} = initial concentration of ligand on the pore wall, g/(cm^3 matrix)
q_{gdt} = concentration of bound ligand-ligate, g/(cm^3 matrix)
q^*_{gdt} = concentration of bound ligand-ligate at equilibrium, g/(cm^3 matrix)
D = diffusion coefficient of the ligate, cm^2/s
Da = Damköhler number as defined by Eq. 9, dimensionless
k_a = associative constant, $cm^3/(g \cdot s)$
k_d = dissociative constant, L/s
K_d = apparent dissociation equilibrium constant, g/cm^3
L = membrane thickness, cm
Ld = Ligand number, $(1-\epsilon)\, q^o_{gd}/(\epsilon C_o)$, dimensionless
ΔP = pressure drop across the membrane, $dyne/cm^2$
Pe_r = Peclet number in the r direction, $(r_o^2/D)/(L/U_o)$, dimensionless
Pe_z = Peclet number in the z direction, $(L^2/D)/(L/U_o)$, dimensionless
Q = mass flow rate of the feed, g/s
Q_v = volumetric flow rate of the feed, cm^3/s
r = radial direction, cm
r_o = membrane mean pore radius, cm
r' = dimensionless r direction
R_a = interface adsorption rate, g/(s·cm^3 solution) by Eq. 2
Re = Reynolds number ($= 2r_o U_o \rho/\mu$), dimensionless
t' = mean residence time of the fluid, s
U = linear velocity of the fluid, cm/s
U_o = average linear velocity of the fluid, cm/s
U' = dimensionless linear velocity of the fluid
V = pore volume, cm^3
z = axial (fluid-flow) direction, cm
z' = dimensionless z direction

Greek letters

ϵ = membrane porosity, dimensionless
θ = dimensionless time
μ = fluid viscosity, dyne·s/cm^2
ρ = fluid density, g/cm^3
ϕ = fractional saturation of ligand, dimensionless

Literature Cited

Afeyan, N. B., S. P. Fulton, N. F. Gordon, I. Mazsaroff, L. Várady, and F. E. Regnier, "Perfusion Chromatography Approach to Purifying Biomolecules," *Bio/Technol.*, **8**, 203 (1990).

Arnold, F. H., and H. W. Blanch, "Analytical Affinity Chromatography II. Rate Theory and the Measurement of Biological Binding Kinetics," *J. Chromatogr.*, **355**, 13 (1986).

Bird, R. B., W. E. Steward, and E. N. Lightfoot, *Transport Phenomena*, Wiley, New York (1960).

Brandt, S., R. A. Goffe, S. B. Kessler, J. L. O'Connor, and S. E. Zale, "Membrane-based Affinity Technology for Commercial Scale Purifications," *Bio/Technol.*, **6**, 779 (1988).

Burns, M. A., and D. J. Graves, "Continuous Affinity Chromatography using a Magnetically Stabilized Fluidized Bed," *Biotechnol. Progr.*, **1**, 95 (1985).

Carnahan, B., H. A. Luther, and J. O. Wilkes, *Applied Numerical Methods*, Wiley, New York (1969).

Chase, H. A., "Affinity Separations Utilizing Immobilized Monoclonal Antibodies—a New Tool for the Biochemical Engineer," *Chem. Eng. Sci.*, **39**, 1099 (1984).

Chase, H. A., and N. M. Draeger, "Affinity Purification of Proteins using Expanded Beds," *J. Chromatogr.*, **597**, 129 (1992).

Danckwerts, P. V., "Continuous Flow Systems—Distribution of Residence Times," *Chem. Eng. Sci.*, **2**, 1 (1953).

Ernst-Cabrera, K., and M. Wilchek, "Polymeric Supports for Affinity Chromatography and High-performance Affinity Chromatography," *Makromol. Chem., Macromol. Symp.*, **19**, 145 (1988).

Graves, D. J., and Y.-T. Wu, "On Predicting the Results of Affinity Procedures," *Methods Enzymol.*, **34**, 140 (1974).

Hiester, N. K., and T. Vermeulen, "Saturation Performance of Ion-exchange and Adsorption Columns," *Chem. Eng. Progress*, **48**, 505 (1952).

Horstmann, B. J., C. N. Kenney, and H. A. Chase, "Adsorption of Proteins on Sepharose Affinity Adsorbents of Varying Particle Size," *J. Chromatogr.*, **361**, 179 (1986).

Huang, S. H., S. Roy, K. C. Hou, and C. T. Tsao, "Scaling-up of Affinity Chromatography by Radial-flow Cartridges," *Biotechnol. Progress*, **4**, 159 (1988).

Iwata, H., K. Saito, S. Furusaki, T. Sugo, and J. Okamoto, "Adsorption Characteristics of an Immobilized Metal Affinity Membrane," *Biotechnol. Progress*, **7**, 412 (1991).

Janson, J., and L. Ryden, *Protein Purification; Principles, High Resolution Methods, and Applications*, VCH Publishers, New York (1989).

Kim, M., K. Saito, S. Furusaki, T. Sato, T. Sugo, and I. Ishigaki, "Adsorption and Elution of Bovine γ-globulin Using an Affinity Membrane Containing Hydrophobic Amino Acids as Ligands," *J. Chromatogr.*, **585**, 45 (1991).

Liu, H.-C., "Membrane-based Affinity Chromatography—Modeling and Experiments of Lysozyme onto Cibacron Blue Ligand Immobilized on Microporous Cellulose Membranes," PhD Dissertation, University of Cincinnati, Cincinnati, OH (1993).
Luong, J. H. T., A.-L. Nguyen, and K. B. Male, "Affinity Crossflow Filtration for Purifying Biomolecules," *Bio/Technol.*, **5**, 564 (1987).
Miller, I., and J. E. Freund, *Probability and Statistics for Engineers*, 3rd ed., Prentice Hall, Englewood Cliffs, NJ (1985).
Pungor, E., N. B. Afeyan, N. F. Gordon, and C. L. Cooney, "Continuous Affinity-Recycle Extraction: a Novel Protein Separation Technique," *Bio/Technol.*, **5**, 604 (1987).
Thomas, H. C., "Chromatography: a Problem in Kinetics," *Annals of New York Acad. of Sci.*, **49**, 161 (1967).
Wankat, P. C., "Theory of Affinity Chromatography Separations,"*Anal. Chem.*, **46**, 1400 (1974).
Zale, S. E., S. B. Kessler, R. A. Goffe, and S. L. Matson, "Affinity Membranes for Protein Purification," paper presented in North American Membrane Society Second Annual National Meeting, Syracuse, NY (Jan., 1988).

Manuscript received Jan. 11, 1993, and revision received June 3, 1993.